Visualization and Modeling of Inhibition of IL-1β and TNFα mRNA Transcription at the Single-Cell Level

Daniel Kalb[1,+], Huy D. Vo[2,+] , Samantha Adikari[3], Elizabeth Hong-Geller[3], Brian Munsky[2,*], James Werner[1,*]

Abstract

IL-1β and TNFα are canonical immune response mediators that play key regulatory roles in a wide range of inflammatory responses to both chronic and acute conditions. Here we employ an automated microscopy platform for the analysis of messenger RNA (mRNA) expression of IL-1β and TNFα at the single-cell level. The amount of IL-1β and TNFα mRNA expressed in a human monocytic leukemia cell line (THP-1) is visualized and counted using single-molecule fluorescent in-situ hybridization (smFISH) following exposure of the cells to lipopolysaccharide (LPS), an outer-membrane component of Gram-negative bacteria. We show that the small molecule inhibitors MG132 (a 26S proteasome inhibitor used to block NF-κB signaling) and U0126 (a MAPK Kinase inhibitor used to block CCAAT-enhancer-binding proteins C/EBP) successfully block IL-1β and TNFα mRNA expression. Based upon this single-cell mRNA expression data, mathematical models of gene expression indicate that the drugs U0126 and MG132 affect gene activation/deactivation rates between the basal and highly activated states. Models for which the parameters were informed by the action of each drug independently were able to predict the effects of the combined drug treatment. From our data and models, we postulate that IL-1β is activated by both NF-κB and C/EBP, while TNFα is predominantly activated by NF-κB. Our combined single-cell experimental modeling efforts shows the interconnection between these two genes and demonstrates how the single-cell responses, including the distribution shapes, mean expression, and kinetics of gene expression, change with inhibition.

Introduction

Inflammation is a complex biological process that enables the host immune system to counteract potential biothreats. In the inflammatory response, select host receptors react to detrimental stimuli (e.g., pathogens, allergens, toxins, or damaged host cells), which activate various intracellular signaling pathways to secrete cytokines that trigger active recruitment of immune cells to the site of insult/infection.[1] While inflammation is usually beneficial to the host organism when fighting an infection, there is also a wide range of both chronic and acute conditions where remediation of inflammation is necessary for host recovery. For example, in certain viral infections, over-expression of inflammatory cytokines throughout the course of disease progression can lead to a potentially fatal cytokine storm that may be more harmful to the host than the underlying infection.[2] In addition to acute conditions, chronic inflammatory conditions, including

[1]Center for Integrated Nanotechnologies, Los Alamos National Laboratory
[2]Department of Chemical and Biological Engineering, Colorado State University
[3]Bioscience Division, Los Alamos National Laboratory
[+]These authors contributed equally to this work.
[*]Correspondence to: brian.munsky@colostate.edu; jwerner@lanl.gov

rheumatoid arthritis diabetes[3] or persistent pain, can be caused by high concentrations of pro-inflammatory cytokines, such as Interleukin 1β (IL-1β) and Tumor Necrosis Factor α (TNFα).

There are several drugs and medications used to limit or dampen the inflammatory response. The best known of these, non-steroidal anti-inflammatory drugs (NSAIDs**)**, work by inhibiting the activity of cyclooxygenase enzymes (COX-1 and COX-2), which are important for the synthesis of key biological mediators and blood clotting agents.[4] Other drugs may act to inhibit key proteins involved in immune response signaling, such as kinase inhibitors or proteasome inhibitors. For kinase and proteasome inhibitors, these compounds are generally discovered first through binding assays, then studied in vitro by activity assays.[5-8] Cellular assays that monitor the effects of drugs in a more complicated environment generally follow such in vitro studies.[9] In a cellular assay, the effects of a drug can be studied by monitoring the level of inhibition of the target of interest, or may be studied by monitoring changes in a downstream signaling pathway. The role drugs play in dampening mRNA expression can be measured by quantitative PCR of the mRNA[10], through DNA microarrays[11], or by RNA sequencing[12]. While informative, most of these methods explore the response of large, ensemble populations of cells.

In contrast to traditional measurements of gene expression collected as bulk averages from large numbers of individual cells, single-cell techniques have revealed surprisingly rich levels of heterogeneity of gene expression.[13-16] When coupled with appropriate models, these distributions of single-cell gene expression can reveal fundamental information on expression kinetics and gene regulatory mechanisms, which is otherwise lost in the bulk measurements [17, 18]. Methods to measure gene expression in single cells generally rely on either amplification or imaging techniques. There are tradeoffs between the two techniques. Amplification-based methods, such as sequencing and PCR, provide high gene depth (tens-to-hundreds of genes can be analyzed) but can be expensive, generally analyze a small number of individual cells, and obscures spatial information.[19-23] Imaging methods generally utilize fluorescent oligonucleotide probes complementary to the RNA sequences of interest and include techniques such as single-molecule fluorescence in situ hybridization (smFISH)[16, 24, 25] and multiplexed barcode labeling methods.[26-28] Though fewer genes can be analyzed at one time, smFISH is relatively low cost, yields single-molecule resolution without the need for nucleic acid amplification, can readily measure several hundreds to thousands of individual cells, and directly visualizes the spatial location of each RNA copy.

There have been a number of studies that exploit single-cell methods in conjuction with single-cell modeling to study host inflammatory responses. For example, fluorescence flow cytometry was used to study the population switching between effector and regulatory T cells and to develop a computational model describing this dynamic behavior.[29] Application of single-cell RNA sequencing methods led to discovery of bimodal expression patterns and splicing in mouse immune cells.[30] Another study integrated live cell imaging and mathematical modeling to understand the 'analog' NF-κβ response of cell populations under 'digital' single-cell signal activation.[31] Additionally, a model of JAK1-STAT3 signaling was constructed following cell treatment by a JAK inhibitor with validation by wide field fluorescence microscopy.[32] In order to visualize single-cell immune responses, our lab previously used smFISH to monitor the single-cell mRNA expression of two cytokines, IL-1β and TNFα, in a human monocytic leukemia cell line, THP-1, in response to lipopolysacharride (LPS), a primary component of cell walls in Gram

negative bacteria.[33] This work found a broad cell-to-cell heterogeneity in immune cell response to LPS.

Here, we exploit single-cell imaging and modeling methods to visualize and understand the broad distribution of mRNA responses to LPS stimulation in THP-1 immune cells. Moreover, these models were used to describe the effects of specific inflammatory inhibitors on the host immune response. The drugs employed, MG132, a 26S proteasome inhibitor used to block NF-κB signaling[8], and U0126, a MAPK kinase inhibitor known to block CCAAT-enhancer-binding proteins C/EBP[34], were selected for their differing roles in dampening the inflammatory response mediated by two key inflammatory cytokines: IL-1β and TNFα. Our results show that MG132 inhibits both IL-1β and TNFα mRNA expression, while U0126 primarily inhibits IL-1β expression. Models derived for the action of each drug independently can also accurately predict the behavior of the drug effects when applied in tandem. These results and models support the current biological understanding that IL-1β expression is activated by both NF-κB and C/EBP signaling pathways while TNFα is predominantly activated by NF-κB. Notably, we observe that models developed to describe the effect single drugs can accurately predict the effect of drug combinations, paving the way for predictive computational analyses of combination drug therapies.

Methods

Microscopy and Image Analysis

A fully automated microscopy and image analysis routine was used to count and measure single-mRNA molecules as previously described.[33] In brief, a conventional wide-field microscope (Olympus IX71), arc lamp (Olympus U-RFL-T), high NA objective (Olympus 1.49 NA, 100X), 2D stage (Thorlabs BSC102), Z sectioning piezo (Physik Instrumente, PI-721.20) and cMOS camera (Hamamatsu orca-flash 4.0) are used to image single-cell mRNA content. Following image acquisition, a custom Matlab script is used to: 1) automatically find and segment each individual cell based upon the bright-field cell image, the nuclear stain (DAPI), and the smFISH channel, 2) filter and threshold using a Laplacian-of-Gaussian filter (LOG) to find the single-mRNA copies, 3) fit all of the mRNA 'spots' to a 2D Gaussian using a GPU-accelerated algorithm, and 4) assign and count all single mRNA copies within each cell. Single-cell distributions are characterized by both their shapes and their mean values.

Cell Culture

Human monocytic leukemia cells (THP-1, ATCC) were cultured in a humidified incubator with 5% CO_2 at 37°C in R10% medium: RPMI-1640 Medium (with glutamine, no phenol red, Gibco) supplemented with 10% fetal bovine serum (FBS, ATCC). Cells were passaged every 5-7 days and used for experiments from age 60-120 days.

Slide Preparation

Chambered cover-glass slides (#1.0 borosilicate glass, 8 wells, Lab-Tek) were coated with a sterile bovine fibronectin solution (1μg/well, Sigma, diluted in PBS, Gibco) overnight at 4°C. 10^5 THP-1 cells/well were seeded onto fibronectin-coated slides for differentiation with R10% medium containing 100nM PMA (phorbol 12-myristate 13-acetate, Sigma) for 48hrs at 37°C. After differentiation, cells were serum-starved in serum-free RPMI-1640 Medium (no FBS) for 2hrs at 37°C. Cells were pre-treated with inhibitors (MG132, or U0126, or both) for 1hr at 37°C (10μM

each in serum-free RPMI-1640 medium, 200µL/well). Untreated wells were kept in serum-free RPMI-1640 medium for 1hr at 37°C. Cells were then stimulated with a cocktail of 500µg/mL lipopolysaccharide (LPS, isolated from *E.coli* O55:B5, Sigma) and 10µM inhibitors (MG132, or U0126, or both) in R10% medium (200µL/well) for 30min, 1hr, 2hrs, or 4hrs at 37°C. Cells were washed in PBS and fixed in paraformaldehyde (4% solution in PBS (v/v), Alfa Aesar) for 15min at room temperature. Unstimulated cells were washed and fixed at t=0hrs immediately after 1hr inhibitor pre-treatment. After fixation, cells were washed twice in PBS, then permeabilized in 70% ethanol in RNase-free distilled water (v/v) (ThermoFisher) for at least 1hr (or up to 24 hrs) at 4°C. Cells were then washed in RNA FISH Wash Buffer A (Stellaris) for 20min at room temperature before RNA smFISH staining for mRNA.

smFISH Staining for mRNA

Cells were stained with custom-designed RNA FISH probes (Stellaris) for IL-1β and TNFα mRNA. Probes were diluted to 100nM each in RNA FISH Hybridization Buffer (Stellaris) containing 10% formamide (v/v) (ThermoFisher), then incubated on the fixed and permeabilized cells using 100µL/well for 4hrs at 37°C. Staining conditions were made in duplicate on each slide. Following probe hybridization, cells were washed three times in RNA FISH Wash Buffer A for 30min each time at 37°C, stained for 20min at 37°C with 100ng/mL DAPI solution (Life Technologies) in RNA FISH Wash Buffer A for 20min at 37°C, and washed in RNA FISH Wash Buffer B (Stellaris) for 20min at room temperature. Cells were washed once in PBS and stored in 200µL/well SlowFade Gold Anti-Fade Mountant (Life Technologies) diluted 4x in PBS for up to 7 days at 4°C. Unless otherwise specified, all steps were performed at room temperature, incubations were performed using 250µL/well, and washes were performed using 500µL/well.

Stochastic reaction networks for modeling gene expression

The time-varying distributions of mRNA copy numbers observed from smFISH experiments are modeled in the framework of the chemical master equation (CME).[35, 36] This analysis proposes a continuous-time Markov chain in which each discrete state corresponds to a vector of integers that represents the copy number for each chemical species. State transitions correspond to reaction events, each of which is represented by a stoichiometry vector. The probabilistic rate of a reaction event is determined through the propensity functions. The time-dependent probability vector $p(t)$ over all states is the solution of the system of linear differential equations $\frac{d}{dt}p(t) = A(t)p(t)$, where $A(t)$ is the transition rate matrix of the Markov chain. The CME was solved using the Finite State Projection (FSP) approach for marginal distributions.[37] All analysis codes are available at [GitHub Site] (**This will be updated upon submission**).

Parameter fitting

The full single-cell dataset consists of four independent biological replicates, each of which contains measurements of IL-1β and TNFα mRNA copy numbers under four different inhibitor conditions (No inhibitor, with MG132, with U0126, and with both MG132 and U0126) and five measurement time points after LPS stiumulation (0min (untreated), 30min, 1hr, 2hrs, and 4hrs). The 'training' dataset on which our CME model was parameterized consists of measurements made under three conditions (No inhibitor, with MG132, and with U0126). Parameters were estimated by minimizing the weighted sum of Kullback-Leibler divergences from the marginal empirical distributions of single-cell observations to those predicted by the CME model.

Evaluation of this likelihood requires the solutions of the CME, which were obtained using the Finite State Projection (FSP) algorithm.[37] (See SI for more details).

Results

Inhibitor treatments reduce transcription levels of IL-1β and TNFα in THP-1 human monocytic leukemia cells

The single-cell mRNA content of IL-1β and TNFα in THP-1 cells were monitored over time after exposure to LPS and in response to two small molecule inhibitors MG132 and U0126, both alone and in combination. MG132 is a selective inhibitor of the NF-κB pathway, while U0126 inhibits the C/EBP pathway, part of the MAPK signaling cascade. [8, 38, 39] Representative images of gene expression after LPS exposure in the presence and absence of small molecule inhibitors are shown in Figures 1 and 2 for 1 and 2 hours post exposure.

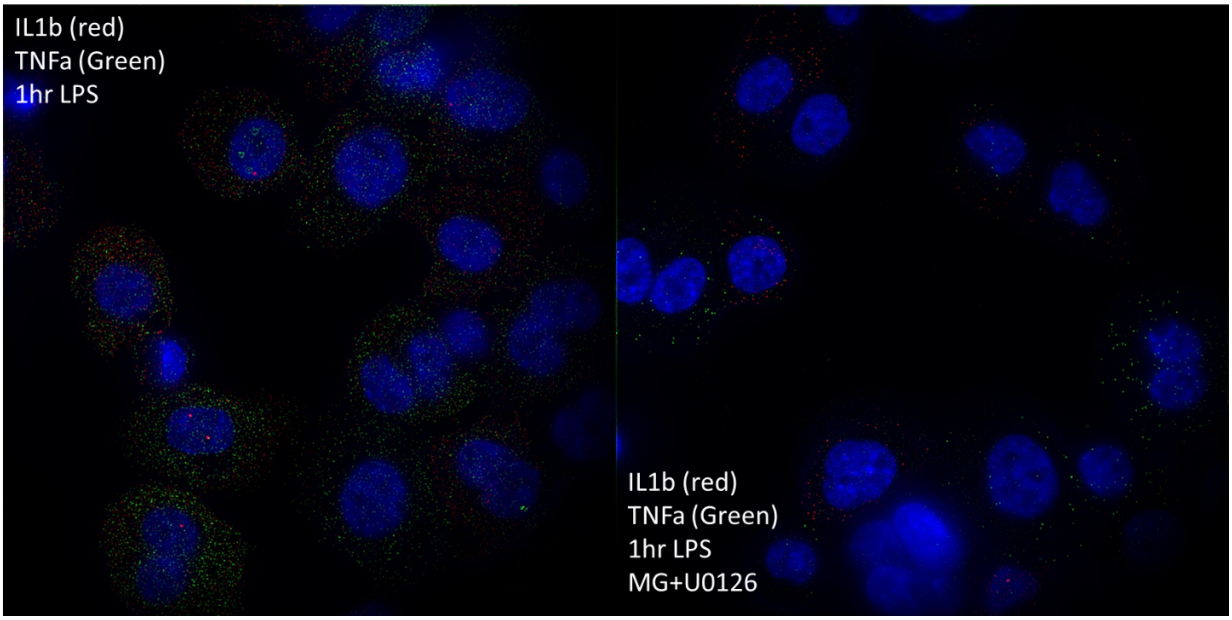

Figure 1. Representative images of IL-1β and TNFα mRNA expression with and without inhibitors at 1hrs LPS exposure. Blue is DAPI-stained nuclei, whereas red spots are individual copies of IL1β and green spots are individual copies of TNFα. Each image is ~130 by 130 μm.

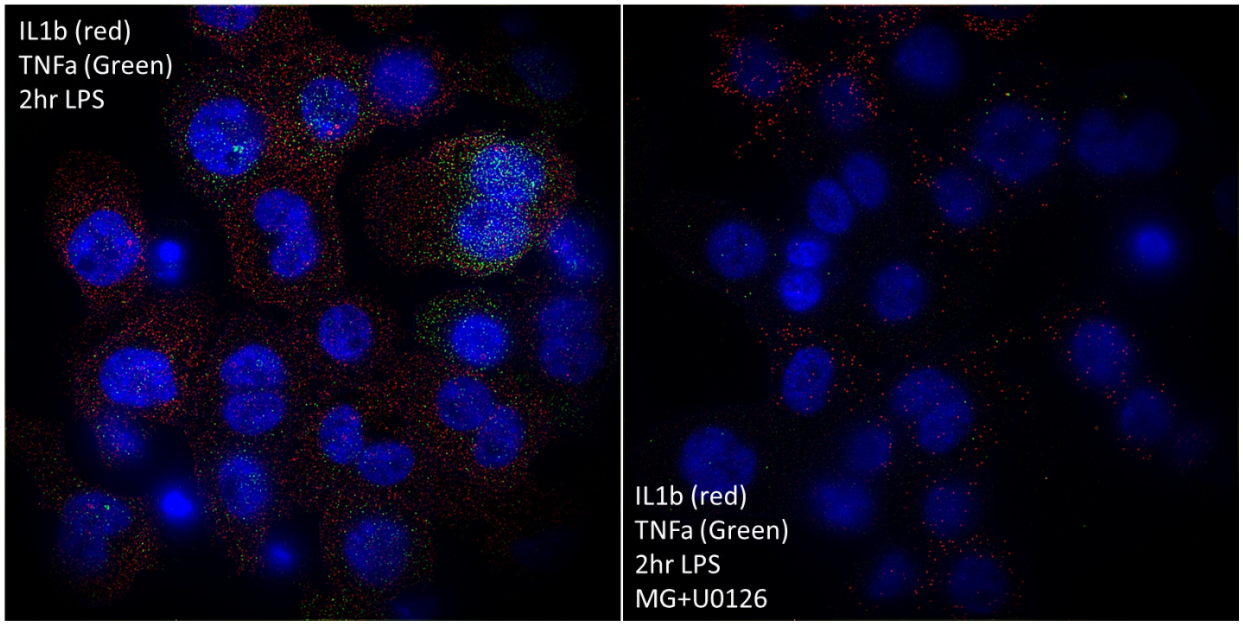

Figure 2. Representative images of IL-1β and TNFα mRNA expression with and without inhibitors at 2 hrs LPS exposure. Images are LOG-filtered to emphasize single mRNA copies that appear as small diffraction limited spots in images. Blue is DAPI-stained nuclei, whereas red spots are individual copies of IL1β and green spots are individual copies of TNFα. Each image is ~130 by 130 μm.

Stochastic models of individual gene expression can fit and predict the probability distribution of transcriptional responses to inhibitor conditions

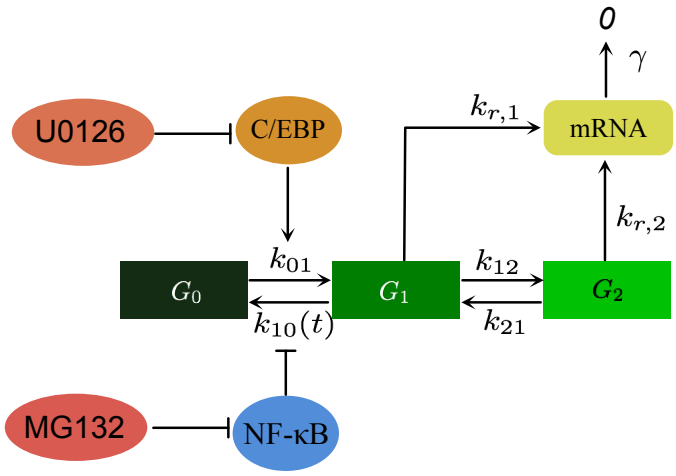

Figure 1. Kinetic model of gene activation. Both TNFα and IL-1β genes can exist in one of three states (off (G0), ready (G1), or on (G2)). mRNA can be transcribed from both the ready and on states, but at a much faster rate from the on state. Forward and reverse transitions between the states occur with the indicated kinetic parameters. The inhibitors U0126 and MG132 affect the transition rates between the off and ready states for the genes. Specifically, U0126 and the kinase C/EBP alter the transition from off to ready, while MG132 and NF-κB alter the transition from ready to off.

A three-state gene expression model was developed to capture the stochastic transcriptional dynamics of the individual genes TNFα and IL-1β (Figure 1). Both TNFα and IL-1β genes can exist in one of three transcriptional states: 'off' (G_0), 'ready' (G_1), and 'on' (G_2). When the gene

is in the 'off' state, no transcriptional activity takes place, whereas when the gene is either 'ready' or 'on', transcription occurs stochastically, with the 'on' state having a much higher transcription rate. The activation of the two genes by C/EBP and NF-κB was modeled via their effects on gene-state transition rates, either increasing the 'off' to 'ready' rate in the case of CEBP or decreasing the 'ready' to 'off' rate for NF-κB. Specifically, the switching rate from G_1 to G_0 was assumed to depend on the time-varying abundance of NF-κB, where NF-κB reduces the rate at which an already transcriptionally active gene switches off. More precisely, the time-dependent deactivation rate is given by $k_{10}(t) = max\left(0, k_{10}^{(a)} - k_{10}^{(b)} NF\kappa B(t)\right)$, where $NF\kappa B(t)$ is the concentration of NF-κB, parametrized by a function of the form

$$NF\kappa B(t) = e^{-r_1 \cdot t}(1 - e^{-r_2 \cdot t}).$$

C/EBP was assumed to exert a constant influence on the rate of switching from G_0 to G_1. This model of NF-κB activation is in general agreement with the literature on NF-κB nuclear localization.[40] The expression dynamics of different genes (IL-1β, TNFα) in response to different treatments (No inhibitors, with MG132, U0126, or both) were described by chemical master equations (CMEs) with the same reactions but different kinetic rate parameters. The effects of inhibitors, when present, were modeled as the reductions to the influence that CEBP or NF-κB exerted on gene activation. The full set of chemical reactions as well as the fitted parameter values are presented in the SI.

The single-cell mRNA distribution shapes of both IL-1β and TNFα in response to LPS (Fig. 4) are indicative of 'bursting' gene expression, characterized by most cells exhibiting lower expression and a long 'tail' of relatively rare high-expressing cells. The distributions of mRNA copies per cell in the presence of the small-molecule inhibitors (Figs.4(B-D) and 4(F-H)) retain their bursting shape (similar to the expression patterns seen with no LPS (Figs. 4A and 4E)). Based upon how the cell-to-cell mRNA distributions change in the presence of the drugs MG132 and U0126, we postulated that these drugs could modulate how NF-κB or C/EBP regulate gene expression. We note that kinetic parameters were determined from the measured mRNA distributions in the drug free and single-drug exposure time-course experiments (Table 1). These parameters then were used to predict the combined drug condition (without any additional fitting of the data), yielding a good approximation of the measured mRNA distributions (Supplementary Figures 1 and 2).

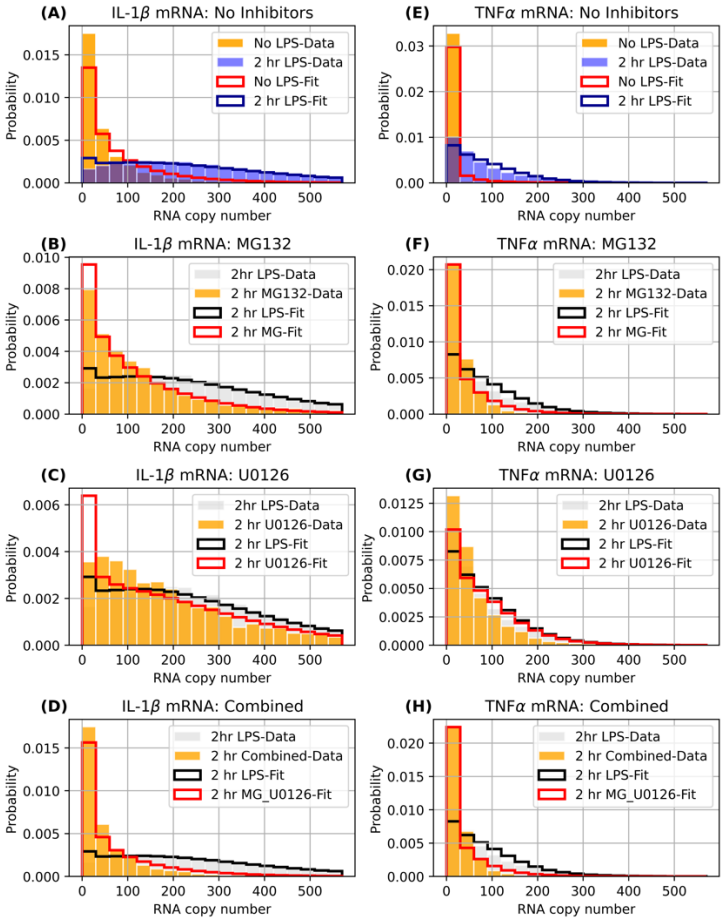

Figure 2. Distributions for single-cell mRNA content. (A-D) Probability distribution (data represented as bars, model fits/predictions as solid lines) for number of IL-1β copies per cell with: (A) 2hr LPS exposure with no inhibitor treatment, (B) 2hr LPS exposure with MG132, (C) 2hr LPS exposure with U0126, and (D) 2hr LPS exposure with U0126 and MG132 combined. (E-H) same as (A-D), but for TNFα. For reference, each panel shows the corresponding mRNA distribution at 2hr LPS exposure with no inhibitor treatment (data in grey, model in black). A-C and E-H show the model fits to data with no inhibitors or a single inhibitor, and D,H show the validation of model predictions for the two inhibitor combination.

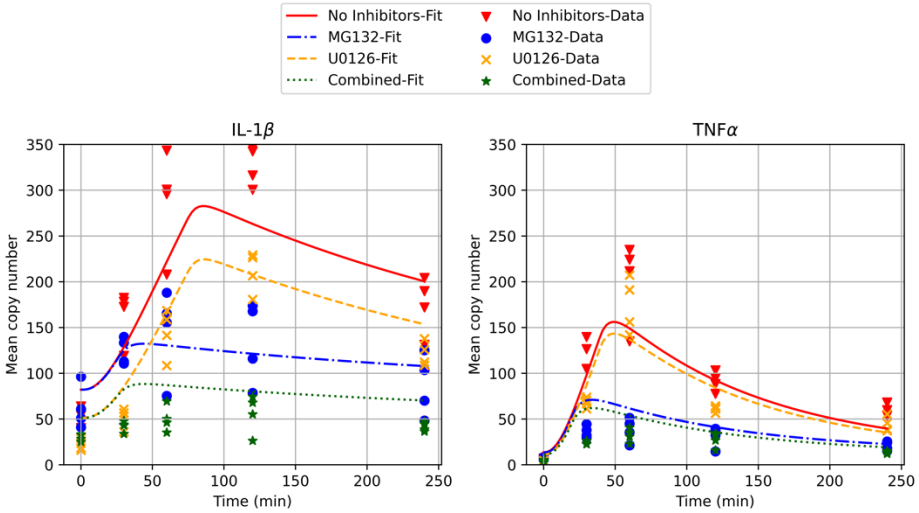

Figure 3. Mean mRNA copies per cell with and without inhibitors over 4hrs of LPS exposure (timepoints 0min, 30min, 1hr, 2hr, and 4hr) estimated from four independent biological replicates per inhibitor condition (markers) and model fits based on the single-gene models (solid and dashed lines).

The mean measured mRNA expression from 0 to 240 min post LPS exposure (as well as model predictions) are plotted in Figure 3. In the absence of inhibitors, the cells show a rapid increase in both IL-1β and TNFα mRNA content following introduction of LPS, with expression peaking at ~325 mRNA copies per cell at 2 hrs and ~200 mRNA copies per cell at 1 hr, respectively. In the presence of inhibitors, we see that IL-1β expression is inhibited by both U0126 and MG132, but with different kinetic trajectories. MG132 treatment dampens IL-1β expression with maximum expression at ~140 mRNA copies per cell at 1 hr. In contrast, U0126 strongly inhibits IL-1β expression at early time points (0-30 min), but is less effective at later time points, with maximal expression at 200 mRNA copies per cell after 120 min. The combination of the two inhibitors results in low expression of IL-1β across all time points, with <50 mRNA copies per cell. For TNFα, MG132 markedly reduces expression from ~200 mRNA copies per cell to <50 mRNA copies per cell at 60 min. Interestingly, U0126 shows very little inhibition of TNFα when used alone. Addition of both inhibitors led to low expression of TNFα, similar to MG132 treatment alone.

	IL-1β	TNFα
r_1	2.61e-03	2.61e-03
r_2	1.26e-04	1.26e-04
k_{01}	8.97e-04	1.18e-03
a_{10}	1.44e-02	8.79e-02
b_{10}	2.10e+03	1.39e+02
k_{12}	6.33e-04	8.60e-04
k_{21}	3.38e-03	2.16e-03
α_0	1.58e-07	1.58e-08
α_1	7.50e-04	2.89e-02
α_2	4.41e-01	2.80e-01
γ	5.90e-05	1.44e-04
b_{10}-MG132	4.04e+00	1.42e+01
k_{01}-U0126	5.54e-04	9.80e-04

Table 1 Fitted parameters for the single-gene models. interpreted as average per second rates of the chemical reactions. These are obtained by fitting the model-predicted distributions of RNA copy number to data collected under three inhibitor conditions (no inhibitors, MG132, and U0126).

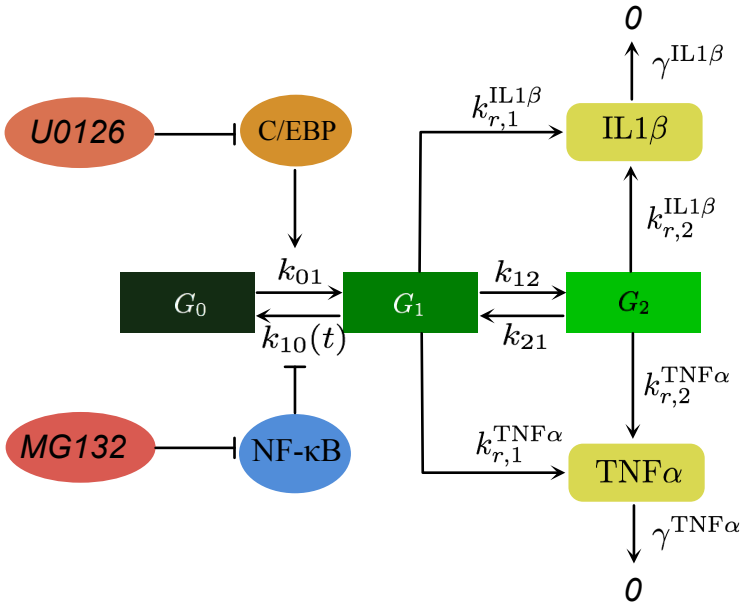

Figure 4. Coupled kinetic model of gene activation. The combined state of TNF-α and IL-1β genes can be in one of three states (G_0, G_1, or G_2). Transcription is activated at different levels on the G_1 and G_2, while G_0 assumes a low basal transcription activity. Forward and reverse transitions between the states occur with the indicated kinetic parameters. The inhibitors U0126 and MG132 affect the transition rates between the off and ready states for the genes. Specifically, U0126 and the kinase C/EBP alter the transition from off to ready, while MG132 and NF-κB alter the transition from ready to off.

A coupled stochastic transcription model can fit and predict the simultaneous response of both TNFα and IL-1β genes to inhibitor conditions

While the single-gene model introduced in the previous section can accurately reproduce the marginal distributions for the number of TNFα or IL-1β transcripts per cell (Figs. 4 and 5), these independent models cannot explain the observed correlation between the two mRNA species (See Fig. 8 and Supplementary Fig. S3 for plots of the joint gene distributions). Therefore, we sought an equally simple, but coupled model to capture the joint response of both genes (model shown schematically in Figure 4). Inspired by the strong similarity in parameters (Table 1) for the models when fit to the marginal distributions, as well as strong correlations in the TNFα and IL-1β single-cell data, we hypothesized a coupled-gene model that assumes that cells switch stochastically between three cellular states, G_0, G_1, and G_2, which control the activity of both genes simultaneously. Specifically, G_0 denotes a joint state in which both genes are at low basal transcription rates, while the G_1, and G_2 allow RNA molecules to be transcribed from both genes simultaneously, albeit at different rates. Similar to the single-gene model, we modeled inhibitor effects in terms of their modulation of the rate by which the cells switch between the G_0 and G_1 states. Upon preliminary fitting of the individual and joint first and second statistical moments, we found that the coupled model could simultaneously capture the mean responses of both genes and also explain the observed positive covariance between the two genes.

We next fit the coupled-gene model to the observed mRNA histograms of both genes at all five different time points, either without inhibitors or with single inhibitors (MG132 or U0126). We then combined the parameters from these fits to predict the response to the tandem inhibitor condition (both MG132 and U0126). The predicted results for the means and second-order summary statistics are plotted in Figure 5, and the model *predictions* for the joint distribution of

IL-1β and TNFα mRNA copy numbers are plotted in Figure 6. It is somewhat surprising that the model parameters, which were obtained by matching only the marginal distributions of individual mRNA species, yield relatively good predictions for the joint response under different treatments.

Table *2* shows the best-fit parameters upon constraining the model to simultaneously match the marginal distributions of TNFα and IL-1β. In the context of the reaction network model (Figure 4), these parameters allow us to propose several potential mechanisms for the observed gene regulation dynamics. First, in the absence of NF-κB, the average rate for the cell to escape the basal state (k_{01}) is over 33 times smaller than the average rate to revert back into inactivation ($k_{10}^{(a)}$) or either of the transition rates between states G_1 and G_2. This means that over the long timespan prior to LPS stimulation, cells are most likely to be in the inactive G_0 state. However, with an average burst refractory period of $1/k_{01}^{a} \approx 909$ seconds, there are occasional bursts of transcripts for both TNFα and IL-1β in a given cell. The majority of these bursts only last for an average burst duration of about $1/k_{10}^{a} \approx 29$ seconds. Although the average burst refractory period and duration are the same for both genes, the basal transcription rate of IL-1β is several orders of magnitude higher than TNFα, which accounts in part for the steady state difference in mean expression between the two genes. This effect is amplified by the fact that IL-1β mRNA (model-estimated half life of 247 minutes) degrades approximately five times slower on average than do TNFα mRNA (model-estimated half-life of 49 minutes).

Upon LPS stimulation, the model suggests that a pulse of NF-κB temporarily decreases the k_{10} rate to zero for approximately $\tau_{\text{NF-κB}} = 46$ minutes (or approximately 0.65 burst refractory periods). This period of time is sufficient for a fraction of approximately $1 - \exp(-k_{01} \times \tau_{\text{NFκB}}) \approx 0.95$ of inactive cells to reach the active state. The effect of this NF-κB signal pulse substantially disrupts the equilibrium between the G_0 and G_1 states and also allows the cells to spend a much longer time in the activated G_1 state with a far greater probability to continue on into the G_2 state. Figure 7 illustrates the expected cell state versus time after addition of the LPS stimulation. According to the model, the cell activation states are relatively short lived, lasting only a little longer than the NF-κB signal pulse itself. However, despite the short-lived activation of the cells, the relatively slow degradation rates for the two mRNA species assures that mRNA transcripts persist for much longer than either the activating signal or the cell activation states. The difference in the degradation rates between the two mRNA species then contributes to a higher peak and slower decay in the mean response of IL-1β in comparison to TNFα, as seen in Figure 5 (panels A and B).

The coupled-gene model also helps to explain the transcription response after treatment with the two anti-inflammatory drugs. When MG132 is added, the effect of the NF-κB signal is substantially reduced. As a consequence, the burst refractory period of the cells is the same, but activated cells switch off relatively rapidly, as compared to the drug-free LPS response, with the deactivation rate $k_{10}(t)$ returning to its full strength after only about 20 minutes (a little less than half of the 46 minutes estimated for the untreated cells). This reduction in the NF-κB signal results in substantially fewer mRNA molecules being produced for either gene. The inhibitor U0126, on the other hand, increases the burst refractory period by a factor of 1.3, which also results in a slightly higher chance that the cell will not activate during the short period of elevated NF-κB and will therefore produce no mRNA. The combined effects of both drugs then deflate the production rate of mRNA further, resulting in almost no difference in the mean copy numbers of both mRNA

species before and after LPS addition (Figure 5, green dotted lines). Figure 7 illustrates the effect of inhibitors on the combined gene states, where the presence of inhibitors reduces the average cell state index, increasing the chance that the cell is in the inactive state.

	No Inhibitors	MG	U0126	Combined
r_1	2.61E-03	2.61E-03	2.61E-03	2.61E-03
r_2	1.10E-04	1.10E-04	1.10E-04	1.10E-04
k_{01}	1.10E-03	1.10E-03	8.24E-04	8.24E-04
a_{10}	3.38E-02	3.38E-02	3.38E-02	3.38E-02
b_{10}	1.99E+02	7.28E+00	1.99E+02	7.28E+00
k_{12}	7.89E-04	7.89E-04	7.89E-04	7.89E-04
k_{21}	2.65E-03	2.65E-03	2.65E-03	2.65E-03
$\alpha_0^{(IL1\beta)}$	1.21E-06	1.21E-06	1.21E-06	1.21E-06
$\alpha_1^{(IL1\beta)}$	1.80E-03	1.80E-03	1.80E-03	1.80E-03
$\alpha_2^{(IL1\beta)}$	3.73E-01	3.73E-01	3.73E-01	3.73E-01
$\alpha_0^{(TNF\alpha)}$	6.90E-08	6.90E-08	6.90E-08	6.90E-08
$\alpha_1^{(TNF\alpha)}$	2.46E-02	2.46E-02	2.46E-02	2.46E-02
$\alpha_2^{(TNF\alpha)}$	4.01E-01	4.01E-01	4.01E-01	4.01E-01
$\gamma^{(IL1\beta)}$	4.67E-05	4.67E-05	4.67E-05	4.67E-05
$\gamma^{(TNF\alpha)}$	2.34E-04	2.34E-04	2.34E-04	2.34E-04

Table 2. Fitted parameters for the coupled-gene models (cf. Figure 4), interpreted as average per second rates of the chemical reactions. These are obtained by fitting the model-predicted marginal distributions of both RNA species to data collected under three inhibitor conditions (no inhibitors, MG132, and U0126).

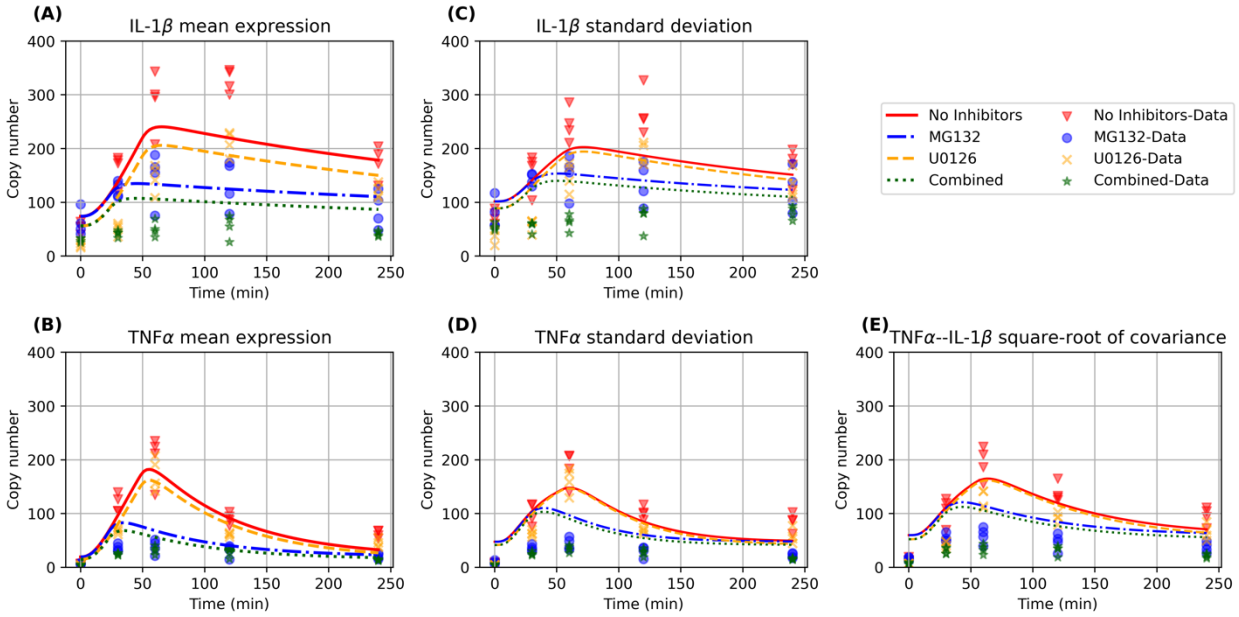

*Figure 5. Coupled-gene model fits for the joint summary statistics of IL-1β and TNFα. **(A-B):** Mean mRNA copies per cell with and without inhibitors over 4hrs of LPS exposure (timepoints 0min, 30min, 1hr, 2hr and 4hr) measured from four biological replicates (markers) and predictions from the coupled-gene model (lines). **(C-E):** The time-dependent second-order summary statistics of IL-1β and TNFα predicted by the coupled-gene model (lines) versus sampled measurements from four biological replicas(markers). These include the time history of IL-1β standard-deviation (C), TNFα standard deviation D), and square root of IL-1β--TNFα covariance (E).*

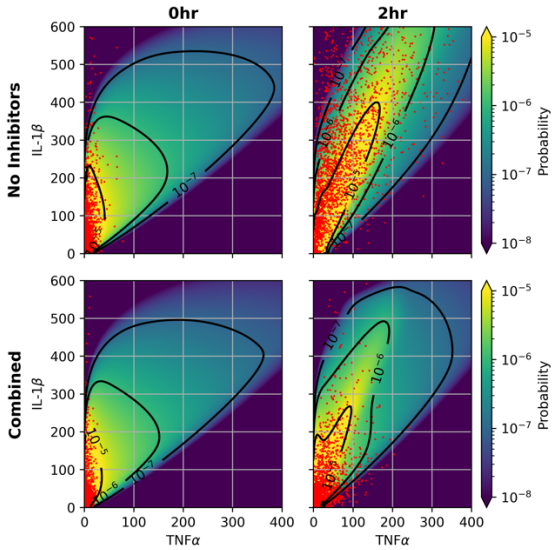

Figure 6 Joint transcriptional response of IL-1β and TNFα without inhibitors (top row) and with combined inhibitors (bottom row) at measurement times 0 hr (left) and 2 hr after LPS addition (right). The model predicted joint distribution of the mRNA species is represented by the heatmap and with annotated contours at three levels 10^{-5}, 10^{-6}, and 10^{-7} . The data points from all biological replicates are represented as red dots.

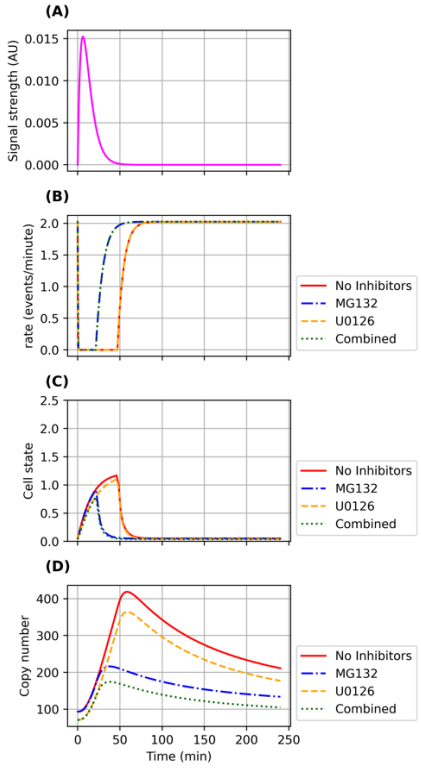

*Figure 7. The downstream influence of NF-κB. **(A):** Signal strength of NFκB in the nucleus in arbitrary units (AU). **(B):** The time-varying rates for switching off transcription activities, under four different inhibitor conditions (No inhibitors, MG132, U0126, both MG132 and U0126). **(C):** Plot of mean cell state under four different inhibitor conditions (No inhibitors, MG132, U0126, both MG132 and U0126). The average cell state is defined by the mathematical expression* $0 \times P(\text{cell state} = C_0) + 1 \times P(\text{cell state} = C_1) + 2 \times P(\text{cell state} = C_2)$. ***(D):** Plot of mean total mRNA copy number under four different inhibitor conditions (No inhibitors, MG132, U0126, both MG132 and U0126).*

Discussion

Single-cell measurements allow for a more complete description and characterization of gene expression kinetics and regulatiory mechansims. Applying single-cell measurement techniques, we have demonstrated that gene transcription heterogeneity of two key immune response genes, IL-1β and TNFα, occurs to a surprising extent within a seemingly uniform cell population following an immune assault. Such measurements of cell-to-cell distribution can be more informative than average values obtained from bulk measurements. For example, cells in the tail of the distribution may ultimately dictate the fate of disease progression rather than the average response, such as in the case of highly stimulated cells that lead to a cytokine storm. This is analogous to understanding how certain individuals (such as super-spreaders) may dictate the pathway of an epidemic more than average R_0 values.[41] Here we show that IL-1β and TNFα genes, while upregulated upon bacterial LPS exposure, can be suppressed at the transcriptional level by the inhibitors MG132 and U0126. Interestingly, each of these inhibitors has a different kinetic effect. U0126 inhibits early IL-1β expression, while MG132 causes a delayed inhibition pattern, suggesting that C/EBP signaling occurs prior to NF-κB activity, in response to LPS (see Figure 1). Additionally, we show that TNFα is predominantly and rapidly inhibited by MG132 treatment, suggesting that NF-κB is the primary upstream regulator of TNFα expression in response to LPS.

To describe these results, we have presented herein a regulatory model for IL-1β and TNFα in THP-1 immune cells. We found the time-course of the cell-to-cell distribution of transcript copy numbers for Il-1β and TNFα could be adequately represented by a stochastic model having three states for gene transcription. Moreover, the effects of anti-inflammatory drugs MG132 and U0126 on the mRNA copy numbers of these two genes could be captured with this three state model. While the kinetic model was fit to data for each drug acting independently, this model was able to predict the data well for the combined drug treatment. Our results suggest that a better mechanistic understanding of inhibitor activity on pro-inflammatory cytokines based on single-cell measurements can eventually lead to more effective combination therapies against chronic and acute inflammatory diseases.

While beyond the scope of the current efforts, our results hold open the possibility of predictive kinetic modeling for combination therapies. We note that while there are possible ways to extend the model proposed in this study to describe the joint expression of both IL-1β and TNFα, the large state space required to analyze the joint expression of more than two mRNA species, coupled with the complexity of integrating time-varying kinase signals, poses a prohibitive challenge for current computational tools. Advances in high performance FSP-based inference methods (e.g., [42]) may potentially allow us to tackle the joint modeling approach in future work. Overall, this study emphasizes the need for further use of single-cell measurements to understand gene responses in order to identify outlier cells and capture full distributions.[43] Single-cell gene expression measurements combined with the appropriate model could provide otherwise overlooked insights into the kinetics, spatial distribution, and regulatory mechanisms of any number of genes.

Acknowledgements

DK, SA, EH-G, and JHW were supported by the Los Alamos Directed Research and Development (LDRD) program. HV and BM were supported by National Institutes of Health under grant R35 GM124747. This work was performed, in part, at the Center for Integrated Nanotechnologies, an Office of Science User Facility operated for the U.S. Department of Energy (DOE) Office of Science. Los Alamos National Laboratory, an affirmative action equal opportunity employer, is managed by Triad National Security, LLC for the U.S. Department of Energy's NNSA, under contract 89233218CNA000001.

REFERNCES

1. Chen, L., et al., *Inflammatory responses and inflammation-associated diseases in organs.* 2018. **9**(6): p. 7204.
2. Tisoncik, J.R., et al., *Into the eye of the cytokine storm.* J. Microbiol. Mol. Biol. Rev., 2012. **76**(1): p. 16-32.
3. Grishman, E.K., P.C. White, and R.C. Savani, *Toll-like receptors, the NLRP3 inflammasome, and interleukin-1 beta in the development and progression of type 1 diabetes.* Pediatric Research, 2012. **71**(6): p. 626-632.
4. Rao, P. and E.E. Knaus, *Evolution of nonsteroidal anti-inflammatory drugs (NSAIDs): cyclooxygenase (COX) inhibition and beyond.* Journal of Pharmacy Pharmaceutical Sciences, 2008. **11**(2): p. 81-110s.
5. Duan, W., et al., *Anti-inflammatory effects of mitogen-activated protein kinase kinase inhibitor U0126 in an asthma mouse model.* The Journal of Immunology, 2004. **172**(11): p. 7053-7059.
6. Yoshida, T., et al., *Proteasome inhibitor MG132 induces death receptor 5 through CCAAT/enhancer-binding protein homologous protein.* J Cancer research, 2005. **65**(13): p. 5662-5667.
7. Guo, N. and Z. Peng, *MG132, a proteasome inhibitor, induces apoptosis in tumor cells.* J Asia-Pacific Journal of Clinical Oncology, 2013. **9**(1): p. 6-11.
8. Davies, S.P., et al., *Specificity and mechanism of action of some commonly used protein kinase inhibitors.* Biochemical Journal, 2000. **351**: p. 95-105.
9. Han, Y.H., et al., *The effect of MG132, a proteasome inhibitor on HeLa cells in relation to cell growth, reactive oxygen species and GSH.* J Oncology reports, 2009. **22**(1): p. 215-221.
10. Bougarn, S., et al., *Validation of candidate reference genes for normalization of quantitative PCR in bovine mammary epithelial cells responding to inflammatory stimuli.* J Journal of dairy science, 2011. **94**(5): p. 2425-2430.
11. Kim, H.-J., et al., *Systemic analysis of heat shock response induced by heat shock and a proteasome inhibitor MG132.* 2011. **6**(6).
12. Jiang, K., et al., *RNA sequencing from human neutrophils reveals distinct transcriptional differences associated with chronic inflammatory states.* J BMC medical genomics, 2015. **8**(1): p. 55.
13. Patel, A.P., et al., *Single-cell RNA-seq highlights intratumoral heterogeneity in primary glioblastoma.* 2014. **344**(6190): p. 1396-1401.
14. Kamme, F., et al., *Single-cell microarray analysis in hippocampus CA1: demonstration and validation of cellular heterogeneity.* 2003. **23**(9): p. 3607-3615.
15. Battich, N., T. Stoeger, and L. Pelkmans, *Image-based transcriptomics in thousands of single human cells at single-molecule resolution.* Nature methods, 2013. **10**(11): p. 1127.

16. Raj, A., et al., *Imaging individual mRNA molecules using multiple singly labeled probes.* Nature Methods, 2008. **5**(10): p. 877-879.
17. Munsky, B., G. Neuert, and A. van Oudenaarden, *Using Gene Expression Noise to Understand Gene Regulation.* Science, 2012. **336**(6078): p. 183-187.
18. Munsky, B., et al., *Distribution shapes govern the discovery of predictive models for gene regulation.* Proceedings of the National Academy of Sciences of the United States of America, 2018. **115**(29): p. 7533-7538.
19. Saliba, A.E., et al., *Single-cell RNA-seq: advances and future challenges.* Nucleic Acids Research, 2014. **42**(14): p. 8845-8860.
20. Shalek, A.K., et al., *Single-cell RNA-seq reveals dynamic paracrine control of cellular variation.* Nature, 2014. **510**(7505): p. 363-+.
21. Kalisky, T., P. Blainey, and S.R. Quake, *Genomic Analysis at the Single-Cell Level*, in *Annual Review of Genetics, Vol 45*, B.L. Bassler, M. Lichten, and G. Schupbach, Editors. 2011, Annual Reviews: Palo Alto. p. 431-445.
22. Shalek, A.K., et al., *Single-cell transcriptomics reveals bimodality in expression and splicing in immune cells.* Nature, 2013. **498**(7453): p. 236-240.
23. Macosko, E.Z., et al., *Highly Parallel Genome-wide Expression Profiling of Individual Cells Using Nanoliter Droplets.* Cell, 2015. **161**(5): p. 1202-1214.
24. Femino, A., et al., *Visualization of single RNA transcripts in situ.* Science, 1998. **280**(5363): p. 585-590.
25. Shepherd, D.P., et al., *Counting Small RNA in Pathogenic Bacteria.* Analytical Chemistry, 2013. **85**(10): p. 4938-4943.
26. Chen, K.H., et al., *Spatially resolved, highly multiplexed RNA profiling in single cells.* Science, 2015. **348**(6233): p. 15.
27. Lubeck, E. and L. Cai, *Single-cell systems biology by super-resolution imaging and combinatorial labeling.* Nature Methods, 2012. **9**(7): p. 743-U159.
28. Coskun, A.F. and L. Cai, *Dense transcript profiling in single cells by image correlation decoding.* Nature Methods, 2016. **13**(8): p. 657-+.
29. Feinerman, O., et al., *Single-cell quantification of IL-2 response by effector and regulatory T cells reveals critical plasticity in immune response.* Molecular systems biology, 2010. **6**(1).
30. Shalek, A.K., et al., *Single-cell transcriptomics reveals bimodality in expression and splicing in immune cells.* 2013. **498**(7453): p. 236-240.
31. Tay, S., et al., *Single-cell NF-κB dynamics reveal digital activation and analogue information processing.* 2010. **466**(7303): p. 267-271.
32. Sobotta, S., et al., *Model based targeting of IL-6-induced inflammatory responses in cultured primary hepatocytes to improve application of the JAK inhibitor ruxolitinib.* Frontiers in physiology, 2017. **8**: p. 775.
33. Kalb, D.M., et al., *Single-cell correlations of mRNA and protein content in a human monocytic cell line after LPS stimulation.* Plos One, 2019. **14**(4): p. 16.
34. Wang, Z., et al., *U0126 prevents ERK pathway phosphorylation and interleukin-1beta mRNA production after cerebral ischemia.* Chinese medical sciences journal=, 2004. **19**(4): p. 270-275.
35. McQuarrie, D.A.J.J.o.a.p., *Stochastic approach to chemical kinetics.* 1967. **4**(3): p. 413-478.
36. Van Kampen, N., *Stochastic processes in physics and chemistry, 3rd edn Amsterdam*. 2007, Netherlands: Elsevier.
37. Munsky, B. and M.J.T.J.o.c.p. Khammash, *The finite state projection algorithm for the solution of the chemical master equation.* 2006. **124**(4): p. 044104.
38. Adamik, J., et al., *Distinct Mechanisms for Induction and Tolerance Regulate the Immediate Early Genes Encoding Interleukin 1 beta and Tumor Necrosis Factor alpha.* Plos One, 2013. **8**(8): p. 17.

39. Matsuo, Y., et al., *Proteasome Inhibitor MG132 Inhibits Angiogenesis in Pancreatic Cancer by Blocking NF-kappa B Activity.* Digestive Diseases and Sciences, 2010. **55**(4): p. 1167-1176.
40. Bagaev, A.V., et al., *Elevated pre-activation basal level of nuclear NF-κB in native macrophages accelerates LPS-induced translocation of cytosolic NF-κB into the cell nucleus.* 2019. **9**(1): p. 1-16.
41. Galvani, A.P. and R.M. May, *Dimensions of superspreading.* Nature, 2005. **438**(7066): p. 293-295.
42. Catanach, T.A., H.D. Vo, and B.J.a.p.a. Munsky, *Bayesian inference of Stochastic reaction networks using Multifidelity Sequential Tempered Markov Chain Monte Carlo.* 2020.
43. Hocine, S., et al., *Single-molecule analysis of gene expression using two-color RNA labeling in live yeast.* Nature methods, 2013. **10**(2): p. 119-121.